

# NeAR: Coupled Neural Asset-Renderer Stack

Hong Li<sup>1,2\*</sup> Chongjie Ye<sup>3,10\*</sup> Houyuan Chen<sup>4</sup> Weiqing Xiao<sup>4</sup> Ziyang Yan<sup>5</sup> Lixing Xiao<sup>6</sup>  
 Zhaoxi Chen<sup>7</sup> Jianfeng Xiang<sup>8</sup> Shaocong Xu<sup>1</sup> Xuhui Liu<sup>2</sup> Yikai Wang<sup>9</sup> Baochang Zhang<sup>2†</sup>  
 Xiaoguang Han<sup>10,3</sup> Jiaolong Yang<sup>11</sup> Hao Zhao<sup>12†</sup>  
<sup>1</sup>BAAI <sup>2</sup>BUAA <sup>3</sup>FNii, CUHKSZ <sup>4</sup>NJU <sup>5</sup>UniTn <sup>6</sup>ZJU  
<sup>7</sup>NTU <sup>8</sup>THU <sup>9</sup>BNU <sup>10</sup>SSE, CUHKSZ <sup>11</sup>MSRA <sup>12</sup>AIR, THU

<https://near-project.github.io/>



Figure 1. **Relightable 3D generation.** Generated assets from casually lit inputs (col. 2) rendered under target lighting (col. 1). Cols. 3-5: traditional Blender rendering (Trellis, Hunyuan3D, ours). Col. 6: our method with neural rendering. Col. 7: GT.

## Abstract

Neural asset authoring and neural rendering have emerged as fundamentally disjoint threads: one generates digital assets using neural networks for traditional graphics pipelines, while the other develops neural renderers that map conventional assets to images. However, the potential of jointly designing the asset representation and renderer remains largely unexplored. We argue that coupling them can unlock an end-to-end learnable graphics stack with benefits in fidelity, consistency, and efficiency. In this paper, we explore this possibility with **NeAR**: a Coupled Neural Asset-Renderer Stack. On the **asset** side, we build on Trellis-style Structured 3D Latents and introduce a lighting-homogenized neural asset: from a casually lit input, a

rectified-flow backbone predicts a Lighting-Homogenized SLAT that encodes geometry and intrinsic material cues in a compact, view-agnostic latent. On the **renderer** side, we design a lighting-aware neural renderer that uses this neural asset, along with explicit view embeddings and HDR environment maps, to achieve real-time, relightable rendering. We validate NeAR on four tasks: (1) G-buffer-based forward rendering, (2) random-lit single-image reconstruction, (3) unknown-lit single-image relighting, and (4) novel-view relighting. Our coupled stack surpasses state-of-the-art baselines in both quantitative metrics and perceptual quality. We hope this coupled asset-renderer perspective inspires future graphics stacks that view neural assets and renderers as co-designed components instead of independent entities.

\*Equal contribution. †Corresponding authors.

## 1. Introduction

Images are determined by the interaction of light with scene geometry, materials, and lighting. Classical computer graphics separates this process into asset authoring, where artists define scene properties, and rendering, where a physically based renderer simulates light transport. While effective, this separation requires substantial manual effort, computationally expensive simulations, and makes inverse reconstruction from real-world images or video challenging. Recent advances in neural graphics [3, 6, 16, 20, 28, 44, 45, 48, 52, 54, 55, 60] address these limitations from two complementary directions: *neural asset authoring* uses generative models [3, 5, 6, 20, 44, 45, 48, 55, 60] to synthesize full 3D assets for traditional pipelines, reducing manual effort, while *neural renderers* map these assets—often converted into intermediate representations such as depth, normals, or shading buffers—directly to images [23, 52, 54], providing a data-driven alternative to analytic rendering and enabling more robust inverse inference.

Despite recent progress in generating 3D assets with PBR materials [3, 5, 6, 20, 44, 45, 48, 55, 60], a fundamental limitation remains: asset generation and neural rendering are typically developed in isolation, with assets created assuming a fixed renderer and renderers trained on static asset distributions. This separation becomes problematic when errors in asset decomposition—such as misidentified albedo or incorrect normal maps—propagate through the rendering pipeline. Because rendering is a nonlinear process, small errors in asset decomposition compound into visible artifacts like baked-in shadows or lighting inconsistencies. Fig. 1 demonstrates this issue: existing methods rendered with traditional physically-based renderers (e.g., Blender) exhibit lighting artifacts and fail to achieve faithful relighting.

To this end, we propose **NeAR**, a *Coupled Neural Asset-Renderer Stack* for single-image relightable 3D generation. Our key insight is to co-design the asset representation and rendering process to enable relighting directly through a shared, lighting-homogenized latent space. On the **asset** side, we introduce a *Lighting-Homogenized Structured 3D Latent (LH-SLAT)*. Unlike standard assets that rely on fragile explicit decomposition, our model lifts the casually lit input into a canonical latent form. As visualized in Fig. 2, this process transforms a shadow-affected representation (Shaded-SLAT) into a clean, homogenized state, effectively suppressing baked-in shadows and unstable highlights while preserving geometric cues. On the **renderer** side, we design a *lighting-aware neural renderer*. Conditioned on a lighting tokenizer, this renderer learns to interpret the homogenized latents and synthesize view-dependent appearance under arbitrary HDR environments via differentiable 3D Gaussian splatting. By unifying the representation, NeAR generates assets that naturally support real-time, high-quality relighting and novel-view syn-

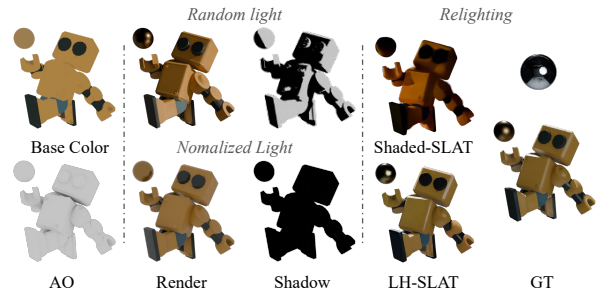


Figure 2. **Lighting homogenization.** Visualization of renders under random lighting and homogenized illumination. Starting from base color and ambient occlusion (AO), we show shaded results under random and canonical lighting, estimated shadows, our lighting-homogenized structured latent (LH-SLAT), and relit outputs compared to ground truth (GT). LH-SLAT suppresses shadows and unstable specularities while preserving geometry-consistent diffuse cues.

thesis with consistent materials across views.

We validate NeAR across four downstream tasks: (1) G-buffer-based forward rendering, (2) random-lit single-image reconstruction, (3) unknown-lit single-image relighting, and (4) novel-view relighting. On benchmarks including Digital Twin Category, Aria Digital Twin, and Objaerse, NeAR achieves state-of-the-art or improved performance over recent neural relighting baselines in both quantitative metrics and perceptual quality, while running at real-time frame rates without per-object optimization.

Our contributions can be summarized as follows:

1. **Coupled neural asset-renderer stack.** We introduce NeAR, an end-to-end learnable graphics stack where the neural asset representation and neural renderer are co-designed for single-image relightable 3D asset generation.
2. **Lighting-homogenized structured neural asset.** We propose a Lighting-Homogenized Structured 3D Latent (LH-SLAT) that suppresses shadows and unstable highlights while preserving geometry-consistent diffuse cues in a compact, view-agnostic 3D latent.
3. **Lighting tokenizer and lighting-aware neural 3D Gaussian renderer.** We design a lighting tokenizer and a lighting-aware neural 3D Gaussian renderer that map LH-SLAT, environment illumination, and view embeddings into a relightable 3D Gaussian field rendered via differentiable Gaussian splatting.
4. **Extensive evaluation and real-time performance.** We demonstrate on multiple datasets and tasks that NeAR delivers state-of-the-art or better quality with strong generalization and consistent multi-view rendering, while enabling real-time feed-forward inference.

## 2. Related Works

### 2.1. Image relighting and inverse rendering

Image relighting and inverse rendering lie at the intersection of geometry, material estimation, and light transport and have been studied from both physics-driven and data-driven perspectives [16]. Classical inverse rendering methods (e.g., SIRFS) recover interpretable PBR maps (albedo, roughness, normals) via optimization and hand-crafted priors [1]. These pipelines are interpretable and editable, but the inverse problem is highly ill-posed in real scenes: shadows, inter-reflections and view-dependent highlights easily bias the recovered materials and produce baked-in artifacts under re-rendering.

Recent learning-based approaches generally fall into two categories. The first focuses on physically-structured decomposition [10, 23, 60]. Although decomposition yields interpretable assets, accurate regression from casual single-view inputs often necessitates multi-view data or costly per-object optimization to resolve ambiguities. The second category targets direct, diffusion-based 2D relighting [11, 28, 52, 56]. Methods like DiLightNet and IC-Light exploit diffusion priors to produce high-fidelity relit images with fine-grained control. However, these approaches are typically computationally expensive, stochastic, and operate in 2D, failing to guarantee multi-view consistency for 3D applications.

In this work we take a middle path: instead of directly solving a brittle PBR inversion or relying on black-box diffusion sampling, we first homogenize the input illumination into a canonical representation (LH-SLAT) and then synthesize a relightable 3D field in a feed-forward manner. This homogenize-then-synthesize strategy stabilizes downstream decoding and improves controllability.

### 2.2. Generative 3D Priors and Representations

Diffusion priors and score-distillation sampling (SDS) have catalyzed rapid progress in text-to-3D and image-to-3D generation [34, 38, 40, 47]. While SDS-based methods transfer 2D generative knowledge to 3D effectively, they suffer from slow iterative optimization. Consequently, recent works have shifted toward feed-forward 3D reconstruction models trained on large-scale 3D datasets [14, 45, 55]. Specifically, Trellis [45] utilizes Structured 3D Latents (SLAT) to compress complex geometry and appearance into sparse tokens, enabling efficient decoding.

Concurrently, 3D Gaussian Splatting (3DGS) [18] has emerged as a rasterization-friendly representation supporting real-time differentiable rendering. While current feed-forward models (like LRM or Trellis) excel at geometry, they typically bake lighting into the texture, limiting downstream utility. Our method builds upon the efficiency of SLAT and 3DGS but fundamentally redesigns the genera-

tion process. We introduce a *lighting-homogenized* variant of SLAT and a custom neural decoder, replacing static texture prediction with a relightable neural field.

### 2.3. Relightable 3D asset synthesis

Producing relightable 3D assets requires models to represent both intrinsic surface properties and lighting-dependent transport (shadows, speculars, interreflections). Prior works condition NeRFs, Gaussian splats or meshes on lighting inputs to enable relighting-aware outputs [2, 12, 16, 21, 33, 36, 46, 51, 59]. Many approaches either use volumetric neural renderers that are costly at inference, or attempt to estimate PBR maps without lighting supervision, which leads to poor disentanglement [26, 35, 39]. Some models explore large inverse-rendering architectures to predict PBR properties from sparse views, but computational cost and optimization per-object remain bottlenecks [22, 58]. Recent works [10, 41] employ diffusion models to generate multi-view material maps or multi-view relighted images, followed by 3D reconstruction. However, the absence of explicit 3D constraints in the generation stage makes it difficult to guarantee consistency across views.

In contrast, our *homogenize-then-synthesize* strategy pipeline explicitly removes unstable, scene-specific illumination before decoding. This mitigates ill-posed PBR inversion, enabling a feed-forward decoder to produce relightable 3DGS with real-time consistency. NeAR thus combines the stability of interpretable pipelines with the fidelity of neural rendering.

## 3. Method

### 3.1. Preliminary

**3D Gaussian Splatting (3DGS).** 3DGS [18] represents scenes with anisotropic Gaussians, rendered via splatting and  $\alpha$ -blending:  $C = \sum_{i \in \mathcal{N}} c_i \alpha_i \prod_{j < i} (1 - \alpha_j)$ . Crucially, standard 3DGS models color  $c_i$  using Spherical Harmonics (SH), which inherently bakes static lighting into the representation. To enable relighting, we forego SH and predict color dynamically conditioned on target illumination.

**Structured 3D Latents (SLAT).** Following Trellis [45], we use SLAT to encode 3D assets efficiently. A SLAT  $\mathcal{Z} = \{(z_k, p_k)\}_{k=1}^K$  consists of  $K$  active feature tokens, where each token  $z_k \in \mathbb{R}^D$  is associated with a coordinate  $p_k$  in a sparse voxel grid. This representation focuses capacity on surface regions ( $K \ll N^3$ ) and supports diverse decoding heads. However, standard SLATs blindly encode input appearance—including shadows and highlights. Our goal is to transform  $\mathcal{Z}$  into a *lighting-homogenized* form, canonicalizing the appearance to a uniform illumination while preserving geometry.

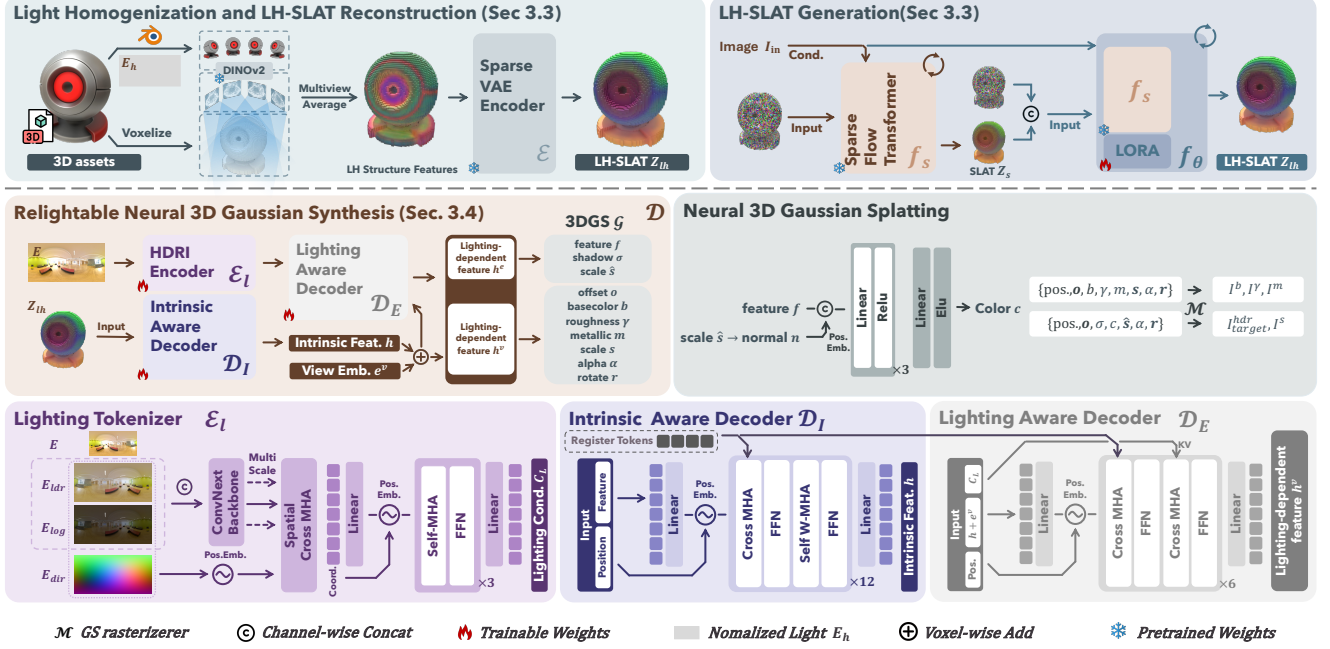


Figure 3. Pipeline of NeAR. Stage 1: *Lighting Homogenization* extracts a Lighting-Homogenized Structured 3D Latent (LH-SLAT) from a casually lit input image. Stage 2: *Reliable 3DGS Synthesis* generates a reliable 3D Gaussian Splatting (3DGS) field conditioned on the LH-SLAT, target illumination, and target viewpoint. The decoded 3DGS encodes geometry, appearance, and light–material interactions, and is rendered into the final relit image.

### 3.2. Overview of NeAR

The challenge in single-image 3D relighting lies in disentangling lighting from intrinsic object properties, since shadows, highlights, and interreflections are inherently entangled with geometry. To avoid unstable PBR inversion and black-box neural generation, we propose a *homogenize-then-synthesize* framework. NeAR first extracts a Lighting-Homogenized SLAT (LH-SLAT) to neutralize lighting effects, then decodes a reliable 3DGS. Our framework consists of two stages:

**Stage 1: Lighting Homogenization.** We first utilize the pre-trained flow model  $f_s$  to map the arbitrarily lit input  $I_{in}$  into an initial shaded SLAT  $Z_s$ . Operating within this sparse voxel space, we employ a LoRA-adapted model  $f_\theta$  to steer the latent representation from  $Z_s$  toward a Lighting-Homogenized SLAT (LH-SLAT)  $Z_{lh}$ :

$$Z_{lh} = f_\theta(Z_s, I_{in}) = f_\theta(f_s(I_{in}), I_{in}). \quad (1)$$

Specifically,  $Z_{lh}$  suppresses the baked-in shadows and highlights inherent in  $Z_s$ , establishing a stable light-homogenized space. This representation preserves essential geometry-material-light interactions, yielding a unified and generalizable foundation for the relighting task.

**Stage 2: Reliable 3DGS Synthesis.** Leveraging the homogenized representation  $Z_{lh}$ , a feed-forward decoder  $\mathcal{D}$  synthesizes a reliable Gaussian field  $\mathcal{G}$ . This process is

conditioned on the target view  $\mathbf{v}_{target}$  and the target illumination  $L_{target}$ , encoded via  $\mathcal{E}_l$ :

$$\mathcal{G} = \mathcal{D}(Z_{lh}, \mathbf{v}_{target}, \mathcal{E}_l(L_{target})). \quad (2)$$

Finally, the relighted image is rendered using a differentiable GS rasterizer  $\mathcal{M}$ :

$$I_{target} = \mathcal{M}(\mathcal{G}, \mathbf{v}_{target}). \quad (3)$$

In the following, we describe Stage 1 (Sec. 3.3) and Stage 2 (Sec. 3.4) in detail.

### 3.3. LH-SLAT Reconstruction & Generation

The first stage generates a Lighting-Homogenized Structured 3D Latent (LH-SLAT)  $Z_{lh}$  from a single input image  $I_{in}$ . This representation serves as a stable, illumination-invariant substrate for downstream synthesis.

**Lighting Homogenization.** We define the homogenized light  $E_h$  as a uniform, white ambient environment illumination. Extracting SLAT features under such lighting captures intrinsic geometric and material cues uncorrupted by transient lighting effects, serving as a robust basis for relighting.

**LH-SLAT Reconstruction.** To train  $f_\theta$ , we prepare paired data  $(I_{in}, Z_{lh})$  via multi-step rendering of 3D assets under homogenized lighting. As shown in Fig. 3 top left corner, we first generate the ground-truth homogenized latents  $Z_{lh}$ : (1) for each 3D asset, we render  $N$  views under

our defined homogenized illumination; (2) we extract dense 2D visual features using a pre-trained DINOv2 model; (3) these features are back-projected into a sparse 3D voxel grid; (4) finally, this sparse grid is compressed by a pre-trained SLAT VAE encoder to obtain  $Z_{lh}$ . Second, to create the corresponding input  $I_{in}$ , we render  $M$  additional images of the same asset under diverse, random lighting conditions and camera poses.

Optionally, for highly reflective materials, we extract Basecolor SLAT  $Z_{bc}$  from multi-view basecolor renderings, concatenating with  $Z_{lh}$  to retain base color information.

**LH-SLAT Generation.** As shown in 3 top right corner, we use a rectified flow model  $f_\theta$  to generate the lighting-homogenized SLAT  $Z_{lh}$  from the input image  $I_{in}$ . The rectified flow model is trained to learn the mapping between the arbitrarily lit image and the corresponding latent representation under our homogenized lighting conditions. Specifically, we utilize a pre-trained SLAT rectified flow model  $f_s$  to generate the shadowed SLAT  $Z_s$  from the input image  $I_{in}$ , and subsequently fine-tune  $f_s$  using LoRA [15] in the sparse voxel space [45] to achieve lighting homogenization. The loss function for training is the conditional flow matching loss  $\mathcal{L}_{stage1}$ :

$$\mathcal{L}_{stage1} = \mathbb{E}_{t, z_0, \epsilon} \|v_\theta(z, Z_s, I_{in}, t) - (\epsilon - z_0)\|_2^2, \quad (4)$$

where  $z(t) = (1 - t)z_0 + t\epsilon$  is the linear interpolation between the data sample  $z_0$  and noise  $\epsilon$ , and  $v_\theta$  approximates the time-dependent vector field. If the optional basecolor SLAT  $z_{bc}$  is used, it is concatenated with  $z_{lh}$  to provide additional color information to the subsequent stage.

### 3.4. Relightable Neural 3DGS Synthesis

The second stage synthesizes a relightable 3D Gaussian Splatting (3DGS) field  $\mathcal{G}$  from LH-SLAT, conditioned on target illumination and viewpoint. Unlike iterative optimization approaches [2, 12], we employ an efficient feed-forward decoder with two sequential modules: the *Intrinsic Aware Decoder (IAD)* and the *Lighting Aware Decoder (LAD)*.

#### 3.4.1. Intrinsic Aware Decoder (IAD)

The IAD, denoted as  $\mathcal{D}_I$ , aims to process LH-SLAT  $Z_{lh}$  and generate a view-independent and illumination-invariant intrinsic feature  $\mathbf{h} = \{(\mathbf{h}_i, \mathbf{p}_i)\}_{i=1}^L$ , where  $\mathbf{h}_i \in \mathbb{R}^{768}$ . This sparse feature field  $\mathbf{h}$  effectively decodes the underlying geometric structure and material properties of the scene. To achieve this, IAD employs a Transformer architecture akin to TRELIS [45], leveraging stacked self-shifted window attention blocks to exploit the inherent locality of structured 3D latent sequences. To further enhance the model’s comprehension of global structural relationships and lighting context, a register cross-attention layer is incorporated into each block. Specifically, 16 learnable register tokens

are appended to each object’s corresponding SLAT token sequences. These tokens encode global scene information and potentially attenuate high-frequency noise within the embeddings [7, 19]. Finally, these register tokens are injected into the decoder via a global cross-attention mechanism, facilitating information exchange between the register tokens and all latent variable tokens, thereby enabling the generation of a coherent and globally consistent intrinsic representation  $\mathbf{h}$ .

#### 3.4.2. Lighting Aware Decoder (LAD)

The LAD, denoted as  $\mathcal{D}_E$ , synthesizes the final lighting-dependent features by injecting view embeddings and environmental lighting conditions, as showed in Fig. 3. .

**Observe View Embedding.** To explicitly model specular highlights that vary with viewing angles, we abandon the commonly used spherical harmonics and instead inject the observed view information into the learning process of LAD from the outset to enhance the model’s perception of specular highlights. Along the camera ray to each voxel  $\mathbf{p}_i$  in the world coordinate system, we record the distance  $x = \{(l_i, \mathbf{p}_i)\}_{i=1}^L$ , where  $l_i \in \mathbb{R}$ , and the ray direction  $\mathbf{d}^w = \{(\mathbf{d}_i^w, \mathbf{p}_i)\}_{i=1}^L$ . We then transform  $\mathbf{d}^w$  to the camera coordinate system using the extrinsic matrix, denoted as  $\mathbf{d} = \{(\mathbf{d}_i, \mathbf{p}_i)\}_{i=1}^L$ , where  $\mathbf{d}_i \in \mathbb{R}^3$ . We apply NeRF positional encoding and learnable positional encoding to  $\mathbf{d}$  and  $l$  voxel-wise, respectively, obtaining the view embedding:

$$\mathbf{e}^v = \{\mathbf{e}^d, \mathbf{e}^l\} = \{(\mathbf{e}_i^d, \mathbf{p}_i), (\mathbf{e}_i^l, \mathbf{p}_i)\}_{i=1}^L, \quad \mathbf{e}_i \in \mathbb{R}^{768}.$$

Then, we add  $\mathbf{e}^d$  and  $\mathbf{e}^l$  voxel-wise to  $\mathbf{h}$  to obtain  $\mathbf{h}^v$ , which serves as the input to LAD.

**Lighting Tokenizer.** We encode the high dynamic range (HDR) environment map  $\mathbf{E}$  into compact lighting conditions using an HDRI encoder  $\mathcal{E}_l$ . Following [13, 16, 23], we decompose  $\mathbf{E}$  into a tone-mapped LDR image  $\mathbf{E}_{ldr}$ , a normalized log-intensity map  $\mathbf{E}_{log} = \log(\mathbf{E} + 1)/\mathbf{E}_{max}$ , and a camera-space direction encoding  $\mathbf{E}_{dir} \in \mathbb{R}^{H \times W \times 3}$ . Unlike prior works that compress the entire map via VAE, we employ a ConvNeXt backbone to extract multi-scale visual features from  $\mathbf{E}_{ldr}$  and  $\mathbf{E}_{log}$ . Crucially, rather than directly compressing  $\mathbf{E}_{dir}$ , we first encode it via NeRF-style positional embedding [30] and fuse it with visual features using **Spatial Cross Attention**. This mechanism acts as a learnable positional encoding, modulating visual features with explicit directional cues. The resulting multi-scale features are concatenated, processed with positional encoding, and passed through self-attention blocks to yield the Lighting Condition Tokens  $C_L \in \mathbb{R}^{4096 \times 768}$ . This design explicitly embeds directional information, facilitating editable lighting directions when switching views.

**LAD Architecture.** LAD primarily consists of stacked cross-attention blocks. The lighting condition  $C_L$  is injected into the intrinsic feature  $\mathbf{h}^v$  via cross-attention layers,



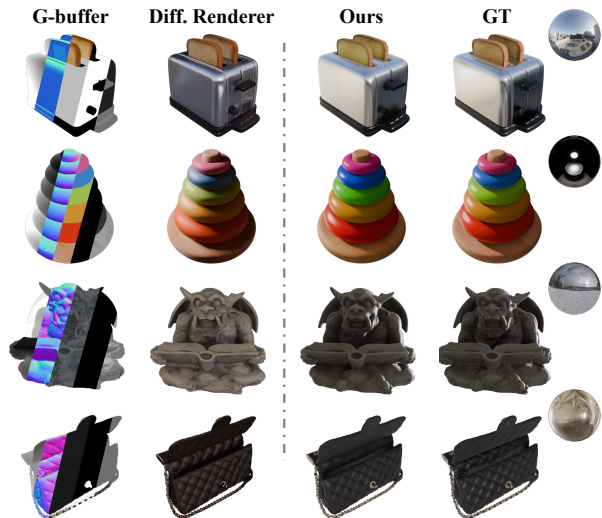


Figure 4. Visual comparison of Diffusion Renderer (with G-buffer) and our LH-SLAT method for image relighting.

rotated environment map. Area light intensities are sampled uniformly between 300 and 700 (units), distances between 5 and 8 units. In the second stage, we re-light objects using randomly rotated environment maps as supervision, with a fixed FOV of  $40^\circ$ . We randomly and uniformly sample 12 camera viewpoints on a sphere of radius 2.0, where each viewpoint is rendered under 16 different illumination conditions. All data generation across both stages utilizes the Blender EEVEE Next engine [42] with raytracing enabled.

**Task Definitions And Baselines.** We evaluate our method on two fundamental tasks: single-view forward rendering and novel view relighting from single-image to Relightable 3D. We evaluate the consistency between the rendered outputs and the ground truth reference images. The former involves single-view forward rendering with input G-buffers (such as normals, material, and depth information), image reconstruction from a single-image under random lighting, and relighting of a single image under unknown lighting. For single-view forward rendering, we compare against recent state-of-the-art neural rendering methods RGB $\leftrightarrow$ X [54], neural-gaffer [16], DiLightNet [52], and Diffusion-render [23]. For novel view relighting, we compare against recent open-source methods that support single-image to 3D generation with PBR materials, including Huyuan3D-2.1 [60] (Hy3D 2.1), MeshGen [6], 3DTopia-XL [5], and SF3D [3].

**Evaluation Metric.** We use PSNR, SSIM [43] and LPIPS [57] to measure the quality of the rendering.

**Evaluation Datasets.** We construct a test set by randomly selecting 800 unseen objects from our training data. To validate generalization capability, we evaluate on out-of-domain datasets: Aria Digital Twin (ADT) [32] and Digital Twin Catalog (DTC) [9], which feature high-fidelity photo-



Figure 5. Visual comparison of image reconstruction.



Figure 6. Visual comparison of relighting.

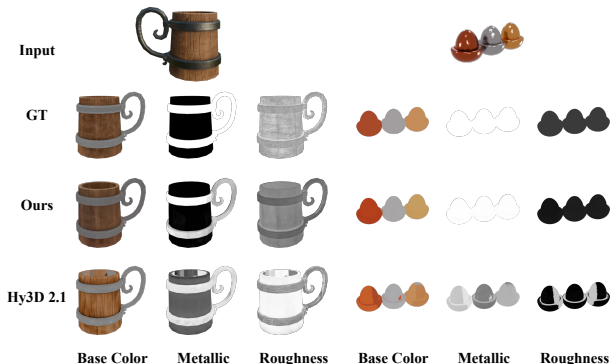


Figure 7. Visual comparison of PBR material estimation.

realistic models with sub-millimeter accuracy. We also incorporate the Glossy Synthetic dataset [24] and additional assets from BlenderKit<sup>1</sup>, modifying rendering nodes to utilize the Principled BSDF shader<sup>2</sup>.

## 4.2. Single-view Forward Rendering

**G-buffers Forward Rendering.** As shown in Fig. 4, we compare against Diffusion Renderer using ground truth G-buffers and LH-Slat, bypassing the single-image-to-intermediate representation step. Our method demonstrates superior accuracy in shadow and highlight distribution (e.g., the toy’s specular highlight and the sculpture’s shadow detail), likely due to our explicit 3D structural information. Furthermore, we accurately capture material reflections of ambient light, as illustrated by the stainless steel. Quantitatively, our method significantly outperforms baselines across four datasets in Tab. 1.

<sup>1</sup><https://www.blenderkit.com/>

<sup>2</sup><https://www.blender.org/>

Table 2. Ablation study on the number of blocks for  $\mathcal{D}_I$  and  $\mathcal{D}_E$ .

Num	PSNR	SSIM	LPIPS	$\mathcal{D}_E$ Param.	FPS
12 + 1	31.56	0.9608	0.0508	12.65M	48
12 + 3	32.35	0.9635	0.0474	31.55M	38
12 + 6	32.54	0.9649	0.0442	59.8M	30
12 + 9	32.56	0.9645	0.0439	88.23M	23
0 + 18	29.43	0.9245	0.0624	173.25M	10

Table 3. Ablation study on decoder input SLAT types.

SLAT types	PSNR	SSIM	LPIPS
shaded	28.95	0.9281	0.0813
base color	30.38	0.9541	0.0564
LH	32.02	0.9631	0.0494
LH + base color	32.54	0.9649	0.0442

**Random-lit Single-image Reconstruction.** As illustrated in Fig. 5, our method achieves higher reconstruction fidelity compared to baselines. Specifically, Diffusion Renderer and RGB-X misestimate materials, while DiLightNet exhibits significant color shifts. Quantitative evaluations in Tab. 1 confirm our method’s advantage across all metrics.

**Unknown-lit Single-image Relighting.** Our method achieves more accurate highlights and color in relit images with unknown lighting, compared to other methods, as shown in Fig. 6. For example, observe the highlights on the speaker cones (first row) and the teapot color (second row). Tab. 1 quantitatively demonstrates the superiority of our method.

**Novel-view Relighting.** We benchmark our full pipeline (single-image to relightable 3D) against state-of-the-art generation methods. While other methods typically reconstruct a mesh and rely on Blender for relighting, we directly generate a relightable 3D Gaussian field. Fig. 1 shows that even with similar geometry, our method achieves more realistic lighting-material interactions than Hunyuan3D. Quantitative results in Tab. 1 demonstrate improvements over existing 3D generation baselines.

**PBR Materials Estimation.** Fig. 7 demonstrates that our method surpasses the open-source SOTA model, Hy3D 2.1, in material recovery. Hunyuan3D relies on multi-view diffusion, which often introduces view-inconsistent artifacts (e.g., blurred edges on the wooden cup). In contrast, our LH-SLAT preserves 3D consistency and retains crucial light-material interaction cues. For instance, Hy3D 2.1 misclassifies wood as metal, resulting in erroneous metallic artifacts on the eggs, whereas our method correctly recovers the material properties.

### 4.3. Ablation Study.

We perform ablation studies on our test set, investigating the Variants of  $\mathcal{D}$  and input SLAT types.

**Variants of  $\mathcal{D}$ .** Tab. 2 indicates that increasing the depth

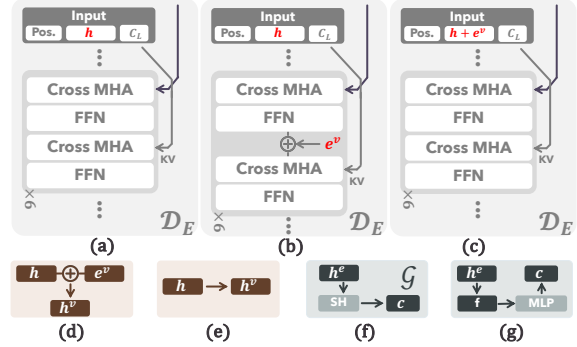


Figure 8. Different designs for the feedforward network  $\mathcal{D}$ .

Table 4. Performance Comparison of Different Architectures.

Arch	PSNR	SSIM	LPIPS
a + e + f	29.82	0.9472	0.0642
a + e + g	30.66	0.9524	0.0515
a + d + g	31.96	0.9597	0.0492
b + d + g	32.43	0.9628	0.0472
c + d + g (ours)	32.54	0.9649	0.0442

of  $\mathcal{D}_E$  improves quality but reduces inference speed; we therefore select 6 layers to strike a balance between efficiency and performance. Relying solely on the LAD  $\mathcal{D}_E$  leads to a significant decline in relighting performance, consistent with [53]. Furthermore, Fig. 8 demonstrates that injecting camera view information to identify which lighting tokens should be attended to, *prior* to lighting baking, significantly enhances relighting results compared to baking global lighting first. This design allows for more effective capture of geometric and lighting variations, boosting the performance of  $\mathcal{D}_E$  (Tab. 4).

**InputTypes.** We analyze the effect of different input latent representations on the decoder  $\mathcal{D}$  in Tab. 3. LH-SLAT, which encodes rich and consistent lighting interaction information, outperforms both Base Color SLAT and Shaded SLAT ( $Z_s$ ). The use of  $Z_s$  complicates relighting due to the entanglement of unknown lighting. However, Base Color SLAT serves as a valuable complement to LH-SLAT; their combination yields the best performance.

## 5. Conclusion

We propose a compact multi-stage framework for relightable 3D generation, enabling consistent high-fidelity reconstruction and realistic relighting. Experiments show improved quantitative and perceptual results over strong baselines, and ablations confirm each component’s contribution. Although evaluated on controlled captures with moderate compute, the approach suggests clear directions for in-the-wild and dynamic scenes and for efficiency and generalization improvements. We hope this work advances practical neural relighting and reconstruction.

## References

- [1] Jonathan T Barron and Jitendra Malik. Intrinsic scene properties from a single rgb-d image. In *CVPR*, 2013. 3
- [2] Zoubin Bi, Yixin Zeng, Chong Zeng, Fan Pei, Xiang Feng, Kun Zhou, and Hongzhi Wu. Gs3: Efficient relighting with triple gaussian splatting. In *SIGGRAPH Asia*, 2024. 3, 5
- [3] Mark Boss, Zixuan Huang, Aaryaman Vasishtha, and Varun Jampani. Sf3d: Stable fast 3d mesh reconstruction with uv-unwrapping and illumination disentanglement. *arXiv:2408.00653*, 2024. 2, 6, 7, 3
- [4] Danpeng Chen, Hai Li, Weicai Ye, Yifan Wang, Weijian Xie, Shangjin Zhai, Nan Wang, Haomin Liu, Hujun Bao, and Guofeng Zhang. Pgsr: Planar-based gaussian splatting for efficient and high-fidelity surface reconstruction. *TVCG*, 2024. 1
- [5] Zhaoxi Chen, Jiayang Tang, Yuhao Dong, Ziang Cao, Fangzhou Hong, Yushi Lan, Tengfei Wang, Haozhe Xie, Tong Wu, Shunsuke Saito, et al. 3dtopia-xl: Scaling high-quality 3d asset generation via primitive diffusion. In *CVPR*, 2024. 2, 6, 7, 3
- [6] Zilong Chen, Yikai Wang, Wenqiang Sun, Feng Wang, Yiwen Chen, and Huaping Liu. Meshgen: Generating pbr textured mesh with render-enhanced auto-encoder and generative data augmentation. In *CVPR*, 2025. 2, 6, 7, 3
- [7] Timothée Darcet, Maxime Oquab, Julien Mairal, and Piotr Bojanowski. Vision transformers need registers. In *ICLR*, 2024. 5
- [8] Matt Deitke, Dustin Schwenk, Jordi Salvador, Luca Weihs, Oscar Michel, Eli VanderBilt, Ludwig Schmidt, Kiana Ehsani, Aniruddha Kembhavi, and Ali Farhadi. Objaverse: A universe of annotated 3d objects. In *CVPR*, 2023. 6
- [9] Zhao Dong, Ka Chen, Zhaoyang Lv, Hong-Xing Yu, Yunzhi Zhang, Cheng Zhang, Yufeng Zhu, Stephen Tian, Zhengqin Li, Geordie Moffatt, et al. Digital twin catalog: A large-scale photorealistic 3d object digital twin dataset. *arXiv:2504.08541*, 2025. 6, 7
- [10] Andreas Engelhardt, Mark Boss, Vikram Voleti, Chun-Han Yao, Hendrik Lensch, and Varun Jampani. Svim3d: Stable video material diffusion for single image 3d generation. In *ICCV*, 2025. 3
- [11] Frédéric Fortier-Chouinard, Zitian Zhang, Louis-Etienne Messier, Mathieu Garon, Anand Bhattad, and Jean-François Lalonde. Spotlight: Shadow-guided object relighting via diffusion. *arXiv:2411.18665*, 2024. 3
- [12] Jian Gao, Chun Gu, Youtian Lin, Zhihao Li, Hao Zhu, Xun Cao, Li Zhang, and Yao Yao. Relightable 3d gaussians: Realistic point cloud relighting with brdf decomposition and ray tracing. In *ECCV*, 2024. 3, 5
- [13] Kai He, Ruofan Liang, Jacob Munkberg, Jon Hasselgren, Nandita Vijaykumar, Alexander Keller, Sanja Fidler, Igor Gilitschenski, Zan Gojcic, and Zian Wang. Unirelight: Learning joint decomposition and synthesis for video relighting. *arXiv:2506.15673*, 2024. 5
- [14] Yicong Hong, Kai Zhang, Jiuxiang Gu, Sai Bi, Yang Zhou, Difan Liu, Feng Liu, Kalyan Sunkavalli, Trung Bui, and Hao Tan. Lrm: Large reconstruction model for single image to 3d. *arXiv:2311.04400*, 2023. 3
- [15] Edward J Hu, Yelong Shen, Phillip Wallis, Zeyuan Allen-Zhu, Yuanzhi Li, Shean Wang, Lu Wang, and Weizhu Chen. LoRA: Low-rank adaptation of large language models. In *ICCV*, 2022. 5, 1
- [16] Haiyan Jin, Yuan Li, Fujun Luan, Yuanbo Xiangli, Sai Bi, Kai Zhang, Zexiang Xu, Jin Sun, and Noah Snavely. Neural gaffer: Relighting any object via diffusion. In *NeurIPS*, 2024. 2, 3, 5, 6, 7
- [17] Damjan Kalajdzievski. A rank stabilization scaling factor for fine-tuning with lora. *arXiv:2312.03732*, 2023. 1
- [18] Bernhard Kerbl, Georgios Kopanas, Thomas Leimkühler, and George Drettakis. 3d gaussian splatting for real-time radiance field rendering. *TOG*, 2023. 3
- [19] Hong Li, Houyuan Chen, Chongjie Ye, Zhaoxi Chen, Bohan Li, Shaocong Xu, Xianda Guo, Xuhui Liu, Yikai Wang, Baochang Zhang, Satoshi Ikehata, Boxin Shi, Anyi Rao, and Hao Zhao. Light of normals: Unified feature representation for universal photometric stereo. *arXiv:2506.18882*, 2025. 5
- [20] Yangguang Li, Zi-Xin Zou, Zexiang Liu, Dehu Wang, Yuan Liang, Zhipeng Yu, Xingchao Liu, Yuan-Chen Guo, Ding Liang, Wanli Ouyang, et al. Triposg: High-fidelity 3d shape synthesis using large-scale rectified flow models. *arXiv preprint arXiv:2502.06608*, 2025. 2
- [21] Zhong Li, Liangchen Song, Zhang Chen, Xiangyu Du, Lele Chen, Junsong Yuan, and Yi Xu. Relit-neuf: Efficient relighting and novel view synthesis via neural 4d light field. In *ACM MM*, 2023. 3
- [22] Zhengqin Li, Dilin Wang, Ka Chen, Zhaoyang Lv, Thu Nguyen-Phuoc, Milim Lee, Jia-Bin Huang, Lei Xiao, Cheng Zhang, Yufeng Zhu, et al. Lirm: Large inverse rendering model for progressive reconstruction of shape, materials and view-dependent radiance fields. *arXiv:2504.20026*, 2025. 3
- [23] Ruofan Liang, Zan Gojcic, Huan Ling, Jacob Munkberg, Jon Hasselgren, Zhi-Hao Lin, Jun Gao, Alexander Keller, Nandita Vijaykumar, Sanja Fidler, et al. Diffusionrenderer: Neural inverse and forward rendering with video diffusion models. *arXiv:2501.18590*, 2025. 2, 3, 5, 6, 7
- [24] Yuan Liu, Peng Wang, Cheng Lin, Xiaoxiao Long, Jiepeng Wang, Lingjie Liu, Taku Komura, and Wenping Wang. Nero: Neural geometry and brdf reconstruction of reflective objects from multiview images. *TOG*, 2023. 6, 7
- [25] Zhuang Liu, Hanzi Mao, Chao-Yuan Wu, Christoph Feichtenhofer, Trevor Darrell, and Saining Xie. A convnet for the 2020s. In *CVPR*, 2022. 2
- [26] Zexiang Liu, Yangguang Li, Youtian Lin, Xin Yu, Sida Peng, Yan-Pei Cao, Xiaojuan Qi, Xiaoshui Huang, Ding Liang, and Wanli Ouyang. Unidream: Unifying diffusion priors for relightable text-to-3d generation. In *ECCV*, 2024. 3
- [27] Ilya Loshchilov and Frank Hutter. Decoupled weight decay regularization. In *ICLR*, 2019. 1
- [28] Nadav Magar, Amir Hertz, Eric Tabellion, Yael Pritch, Alex Rav-Acha, Ariel Shamir, and Yedid Hoshen. Lightlab: Controlling light sources in images with diffusion models. *arXiv:2505.09608*, 2025. 2, 3
- [29] Sourab Mangrulkar, Sylvain Gugger, Lysandre Debut, Younes Belkada, Sayak Paul, and Benjamin Bossan.

- PEFT: State-of-the-art parameter-efficient fine-tuning methods. <https://github.com/huggingface/peft>, 2022. 1
- [30] Ben Mildenhall, Pratul P Srinivasan, Matthew Tancik, Jonathan T Barron, Ravi Ramamoorthi, and Ren Ng. Nerf: Representing scenes as neural radiance fields for view synthesis. *CACM*, 2021. 5
- [31] Maxime Oquab, Timothée Darcet, Théo Moutakanni, Huy Vo, Marc Szafraniec, Vasil Khalidov, Pierre Fernandez, Daniel Haziza, Francisco Massa, Alaaeldin El-Nouby, et al. Dinov2: Learning robust visual features without supervision. *arXiv:2304.07193*, 2023. 3
- [32] Xiaqing Pan, Nicholas Charron, Yongqian Yang, Scott Peters, Thomas Whelan, Chen Kong, Omkar Parkhi, Richard Newcombe, and Yuheng Carl Ren. Aria digital twin: A new benchmark dataset for egocentric 3d machine perception. In *CVPR*, 2023. 6, 7
- [33] Y. Poirier-Ginter, A. Gauthier, J. Phillip, J.-F. Lalonde, and G. Drettakis. A diffusion approach to radiance field relighting using multi-illumination synthesis. *EGSR*, 2024. 3
- [34] Ben Poole, Ajay Jain, Jonathan T Barron, and Ben Mildenhall. Dreamfusion: Text-to-3d using 2d diffusion. *arXiv:2209.14988*, 2022. 3
- [35] Lingteng Qiu, Guanying Chen, Xiaodong Gu, Qi Zuo, Mutian Xu, Yushuang Wu, Weihao Yuan, Zilong Dong, Liefeng Bo, and Xiaoguang Han. Richdreamer: A generalizable normal-depth diffusion model for detail richness in text-to-3d. In *CVPR*, 2024. 3
- [36] Fabio Remondino, Ali Karami, Ziyang Yan, Gabriele Mazzacca, Simone Rigon, and Rongjun Qin. A critical analysis of nerf-based 3d reconstruction. *Remote Sensing*, 2023. 3
- [37] Jay Shah, Ganesh Bikshandi, Ying Zhang, Vijay Thakkar, Pradeep Ramani, and Tri Dao. Flashattention-3: Fast and accurate attention with asynchrony and low-precision. *arXiv:2407.08608*, 2024. 1
- [38] Yichun Shi, Peng Wang, Jianglong Ye, Mai Long, Kejie Li, and Xiao Yang. Mvdream: Multi-view diffusion for 3d generation. *arXiv:2308.16512*, 2023. 3
- [39] Dongseok Shim, Yichun Shi, Kejie Li, H Jin Kim, and Peng Wang. Mvlight: Relightable text-to-3d generation via light-conditioned multi-view diffusion. *arXiv:2411.11475*, 2024. 3
- [40] Jiaxiang Tang, Jiawei Ren, Hang Zhou, Ziwei Liu, and Gang Zeng. Dreamgaussian: Generative gaussian splatting for efficient 3d content creation. *arXiv:2309.16653*, 2023. 3
- [41] Jiapeng Tang, Matthew Lavine, Dor Verbin, Stephan J Garbin, Matthias Nießner, Ricardo Martin Brualla, Pratul P Srinivasan, and Philipp Henzler. Rogr: Relightable 3d objects using generative relighting. In *NeurIPS*, 2025. 3
- [42] Blender Development Team. Eevee release notes for blender 4.2. [https://developer.blender.org/docs/release\\_notes/4.2/eevee/](https://developer.blender.org/docs/release_notes/4.2/eevee/), 2025. 7
- [43] Zhou Wang, Alan C Bovik, Hamid R Sheikh, and Eero P Simoncelli. Image quality assessment: from error visibility to structural similarity. *TIP*, 2004. 7
- [44] Shuang Wu, Youtian Lin, Feihu Zhang, Yifei Zeng, Jingxi Xu, Philip Torr, Xun Cao, and Yao Yao. Direct3d: Scalable image-to-3d generation via 3d latent diffusion transformer. In *NeurIPS*, 2024. 2
- [45] Jianfeng Xiang, Zelong Lv, Sicheng Xu, Yu Deng, Ruicheng Wang, Bowen Zhang, Dong Chen, Xin Tong, and Jiaolong Yang. Structured 3d latents for scalable and versatile 3d generation. *arXiv:2412.01506*, 2024. 2, 3, 5, 6, 1
- [46] Ziyang Yan, Lei Li, Yihua Shao, Siyu Chen, Zongkai Wu, Jenq-Neng Hwang, Hao Zhao, and Fabio Remondino. 3dsce-needitor: Controllable 3d scene editing with gaussian splatting. *arXiv:2412.01583*, 2024. 3
- [47] Ziyang Yan, Nazanin Padkan, Pawel Trybała, Elisa Mariarosaria Farella, and Fabio Remondino. Learning-based 3d reconstruction methods for non-collaborative surfaces—a metrological evaluation. *Metrology*, 2025. 3
- [48] Chongjie Ye, Yushuang Wu, Ziteng Lu, Jiahao Chang, Xiaoyang Guo, Jiaqing Zhou, Hao Zhao, and Xiaoguang Han. Hi3dgen: High-fidelity 3d geometry generation from images via normal bridging. In *ICCV*, 2025. 2
- [49] Vickie Ye, Ruilong Li, Justin Kerr, Matias Turkulainen, Brent Yi, Zhuoyang Pan, Otto Seiskari, Jianbo Ye, Jeffrey Hu, Matthew Tancik, and Angjoo Kanazawa. gsplat: An open-source library for gaussian splatting. *JMLR*, 2025. 1
- [50] Zehao Yu, Torsten Sattler, and Andreas Geiger. Gaussian opacity fields: Efficient adaptive surface reconstruction in unbounded scenes. *TOG*, 2024. 1
- [51] Chong Zeng, Guojun Chen, Yue Dong, Pieter Peers, Hongzhi Wu, and Xin Tong. Relighting neural radiance fields with shadow and highlight hints. In *SIGGRAPH*, 2023. 3
- [52] Chong Zeng, Yue Dong, Pieter Peers, Youkang Kong, Hongzhi Wu, and Xin Tong. Dilightnet: Fine-grained lighting control for diffusion-based image generation. In *SIGGRAPH*, 2024. 2, 3, 6, 7
- [53] Chong Zeng, Yue Dong, Pieter Peers, Hongzhi Wu, and Xin Tong. Renderformer: Transformer-based neural rendering of triangle meshes with global illumination. In *SIGGRAPH*, 2025. 6, 8
- [54] Zheng Zeng, Valentin Deschaintre, Iliyan Georgiev, Yannick Hold-Geoffroy, Yiwei Hu, Fujun Luan, Ling-Qi Yan, and Miloš Hašan. Rgb $\leftrightarrow$ x: Image decomposition and synthesis using material- and lighting-aware diffusion models. In *SIGGRAPH*, 2024. 2, 6, 7, 3
- [55] Longwen Zhang, Ziyu Wang, Qixuan Zhang, Qiwei Qiu, Anqi Pang, Haoran Jiang, Wei Yang, Lan Xu, and Jingyi Yu. Clay: A controllable large-scale generative model for creating high-quality 3d assets. *ACM Transactions on Graphics (TOG)*, 43(4):1–20, 2024. 2, 3
- [56] Lvmin Zhang, Anyi Rao, and Maneesh Agrawala. Scaling in-the-wild training for diffusion-based illumination harmonization and editing by imposing consistent light transport. In *ICLR*, 2025. 3
- [57] Richard Zhang, Phillip Isola, Alexei A Efros, Eli Shechtman, and Oliver Wang. The unreasonable effectiveness of deep features as a perceptual metric. In *CVPR*, 2018. 6, 7
- [58] Tianyuan Zhang, Zhengfei Kuang, Haian Jin, Zexiang Xu, Sai Bi, Hao Tan, He Zhang, Yiwei Hu, Milos Hasan, William T Freeman, et al. Relitlm: Generative relightable radiance for large reconstruction models. *arXiv:2410.06231*, 2024. 3

- [59] Xiaoming Zhao, Pratul P. Srinivasan, Dor Verbin, Keunhong Park, Ricardo Martin Brualla, and Philipp Henzler. IllumiNeRF: 3D Relighting Without Inverse Rendering. In *NeurIPS*, 2024. [3](#)
- [60] Zibo Zhao, Zeqiang Lai, Qingxiang Lin, Yunfei Zhao, Haolin Liu, Shuhui Yang, Yifei Feng, Mingxin Yang, Sheng Zhang, Xianghui Yang, et al. Hunyuan3d 2.0: Scaling diffusion models for high resolution textured 3d assets generation. *arXiv:2501.12202*, 2025. [2](#), [3](#), [6](#), [7](#), [1](#)
- [61] Jialin Zhu, Jiangbei Yue, Feixiang He, and He Wang. 3d student splatting and scooping. In *CVPR*, 2025. [6](#)

# NeAR: Coupled Neural Asset-Renderer Stack

## Supplementary Material

### A. More Implementation Details

#### A.1. Implementation Details

**Training Details.** We conduct all training experiments on four NVIDIA H100 80GB HBM3 GPUs.

In the **LH-SLAT Reconstruction & Generation phase** (§3.3), we fine-tune a rectified flow model equipped with LoRA [15] to normalize shaded SLATs from arbitrary images into LH-SLATs. The goal of this phase is to learn a mapping,  $f_\theta$ , that transforms light-dependent shaded SLAT representations into light-homogenized counterparts. To achieve this efficiently while preserving the prior knowledge of the original flow model  $f_s$  [45], we initialize LoRA using PEFT [29]. We configure LoRA with a rank of 512 and a scaling factor, further integrating rslora [17] to enhance training stability. LoRA adaptors are applied to the query, key, value, and output projection modules within the attention mechanism. We optimize the model using AdamW [27] with a learning rate of  $1 \times 10^{-4}$ . This training phase takes approximately two days to complete.

In the **Relightable Neural 3DGS Synthesis phase** (§3.4), we employ the AdamW optimizer with a batch size of 48. The learning rate is warmed up linearly to  $1 \times 10^{-4}$  over the first 5K steps, followed by a cosine decay schedule. We perform end-to-end joint training on the IAD, LAD, and the Lighting-Aware tokenizer (denoted as  $E_l$ ). To accelerate training, we leverage Flash-Attention 3 [37] and gsplat [49]. The model is trained for 500K iterations across all loss components, requiring approximately 10 days. Additionally, we investigated the incorporation of geometric constraint losses, specifically normal and depth losses. However, we observed that adding these regularizations degraded both convergence speed and rendering quality, suggesting a trade-off between geometric constraints and rendering fidelity within the 3DGS framework [4, 50].

**Inference Details.** Given a single input image  $I_{in}$  with unknown lighting and a target high dynamic range (HDR) environment map  $E$ , our inference pipeline proceeds as follows. Since our method decouples geometry generation from relighting, we first reconstruct a 3D mesh  $m$  from  $I_{in}$  using Hunyuan3D 2.1 (Hy3D 2.1) [60] with default settings. This mesh is then voxelized to provide coordinates for the structurally sparse voxel feature SLAT.

Following Trellis [45], we utilize the pre-trained SLAT flow model  $f_s$  to generate an initial shaded SLAT  $Z_s$  from  $I_{in}$ . Note that  $Z_s$  inherently contains arbitrary lighting information from the input image. To remove these lighting effects, we concatenate  $Z_s$  with noise (matching  $Z_s$  in

shape) along the channel dimension and feed the result into our fine-tuned corrective model  $f_\theta$  to yield the Lighting-Homogenized SLAT (LH-SLAT).

Subsequently, for the target lighting, we pre-process the environment map  $E$  (as detailed in Sec. 3.4.2) and encode it into a lighting condition embedding  $C_L$  using the Lighting-Aware tokenizer  $\mathcal{E}_l$ . The IAD module then processes the LH-SLAT to extract intrinsic features  $h$ . Simultaneously, the LAD  $\mathcal{D}_E$  integrates the viewing direction encoding  $e^v$  and the lighting condition  $C_L$  to predict the 3D Gaussian attributes for the specific view and lighting (Eq. 5). Finally, we render the relit HDR image  $I_{target}^{hdr}$  via gsplat [49]. To align the visual output with standard rendering engines like Blender, we apply AgX tone mapping<sup>3</sup> to convert the HDR result into a low dynamic range (LDR) image.

#### A.2. Network Architectures

**Register Tokens.** Apart from the lighting-aware tokenizer  $\mathcal{E}_l$ , and consistent with [45], our method primarily employs Transformer networks. As depicted in Fig. 3, the IAD  $\mathcal{D}_I$  comprises 3D shifted window multi-head self-attention (3D-SW-MSA) and a feed-forward network (FFN). Addressing the limitation of the naive 3D-SW-MSA design in [45], which computes attention solely within local windows and neglects inter-window information exchange, we introduce learnable register tokens. These tokens interact with all windows via 3D multi-head cross-attention (3D-MCA), serving as a global information bridge to facilitate the model’s learning of global context. The lighting-aware decoder  $\mathcal{D}_E$  receives intrinsic features  $h$ , view encoding  $e^v$ , register tokens, and lighting encoding to generate lighting-dependent features  $h^v$ . Register tokens and lighting encoding are injected into the network via 3D-MCA. Here,  $h$  and  $e^v$  are added in a voxel-wise manner to determine which lighting encoding tokens should be attended to under the current viewpoint. The ablation study on the interaction order of viewpoint and lighting information is illustrated in Fig. 8 and Tab 4.

**Loss Functions.** For the relightable neural 3DGS synthesis stage, we optimize the model using a composite objective function  $\mathcal{L}_{total}$ . This objective is a weighted sum of three primary reconstruction components—HDR reconstruction ( $\mathcal{L}_{recon}$ ), physically-based material supervision ( $\mathcal{L}_{pbr}$ ), and shadow-casting ( $\mathcal{L}_{shadow}$ )—along with regularization terms for Gaussian primitives:

$$\mathcal{L}_{total} = \mathcal{L}_{recon} + \lambda_{pbr}\mathcal{L}_{pbr} + \lambda_{shadow}\mathcal{L}_{shadow} + \lambda_{vol}\mathcal{L}_{vol} + \lambda_\alpha\mathcal{L}_\alpha. \quad (7)$$

<sup>3</sup><https://github.com/iamNCJ/simple-ocio>

In our experiments, we set the weighting hyperparameters to  $\lambda_{\text{pbr}} = 0.3$ ,  $\lambda_{\text{shadow}} = 0.5$ ,  $\lambda_{\text{vol}} = 10,000$ , and  $\lambda_{\alpha} = 0.001$ .

**Reconstruction Loss ( $\mathcal{L}_{\text{recon}}$ ).** We formulate  $\mathcal{L}_{\text{recon}}$  to ensure high-fidelity HDR rendering. Before calculating perceptual metrics, we apply AgX tone mapping to both the rendered HDR image  $I_{\text{target}}^{\text{hdr}}$  and the ground-truth  $I_{\text{gt}}^{\text{hdr}}$ , yielding their LDR counterparts  $\hat{I}_{\text{target}}$  and  $\hat{I}_{\text{gt}}$ . The loss combines an L1 distance in the logarithmic domain for HDR consistency, along with SSIM and LPIPS losses on the tonemapped LDR images for perceptual quality:

$$\begin{aligned} \mathcal{L}_{\text{recon}} = & \mathcal{L}_1(\log(I_{\text{target}}^{\text{hdr}} + 1), \log(I_{\text{gt}}^{\text{hdr}} + 1)) \\ & + 0.2(1 - \text{SSIM}(\hat{I}_{\text{target}}, \hat{I}_{\text{gt}})) \\ & + 0.2\text{LPIPS}(\hat{I}_{\text{target}}, \hat{I}_{\text{gt}}). \end{aligned} \quad (8)$$

**PBR and Shadow Supervision.** To guide the model towards physically plausible decomposition, we impose direct constraints on the intermediate PBR feature maps. The material loss  $\mathcal{L}_{\text{pbr}}$  supervises the base color ( $I^b$ ), roughness ( $I^r$ ), metallic ( $I^m$ ), and shading ( $I^s$ ) maps against their ground truths:

$$\mathcal{L}_{\text{pbr}} = \mathcal{L}_1(I^b, I_{\text{gt}}^b) + \mathcal{L}_1(I^r, I_{\text{gt}}^r) + \mathcal{L}_1(I^m, I_{\text{gt}}^m) + \mathcal{L}_1(I^s, I_{\text{gt}}^s). \quad (9)$$

Similarly,  $\mathcal{L}_{\text{shadow}}$  employs an  $\mathcal{L}_1$  loss to ensure the geometric consistency of cast shadows under novel lighting conditions.

**Regularization.** To prevent the degeneration of Gaussian primitives (e.g., becoming too large or too opaque) during optimization [45], we incorporate a volumetric loss  $\mathcal{L}_{\text{vol}}$  and an opacity loss  $\mathcal{L}_{\alpha}$ :

$$\begin{aligned} \mathcal{L}_{\text{vol}} = & \frac{1}{LK} \sum_{i=1}^L \sum_{k=1}^K \prod s_i^k + \frac{1}{LK} \sum_{i=1}^L \sum_{k=1}^K \prod \hat{s}_i^k, \\ \mathcal{L}_{\alpha} = & \frac{1}{LK} \sum_{i=1}^L \sum_{k=1}^K (1 - \alpha_i^k)^2. \end{aligned} \quad (10)$$

These terms are calculated across the  $L$  active voxels, with each voxel predicting  $K$  Gaussian primitives. Specifically,  $\mathcal{L}_{\text{vol}}$  regularizes the scale components  $s$  from the IAD and  $\hat{s}$  from the LAD simultaneously.

**Lighting Tokenizer** . As illustrated in Fig. 9, the lighting tokenizer  $\mathcal{E}_l$  is primarily designed to process and inject lighting information into the network for relighting purposes, while also effectively perceiving rotations in the ambient lighting. Similar to Neural Graffer and Diffusion Renderer, as depicted in Fig. 9 (a), our approach leverages the  $E_{\text{hdr}}$  and  $E_{\text{log}}$  components of the environment map  $E$  to provide lighting color characteristics. Neural Graffer encodes the environment map into an image latent space via a pre-trained image VAE, whereas Diffusion Renderer employs a video VAE model to compress  $E_{\text{hdr}}$ ,  $E_{\text{log}}$ , and  $E_{\text{dir}}$

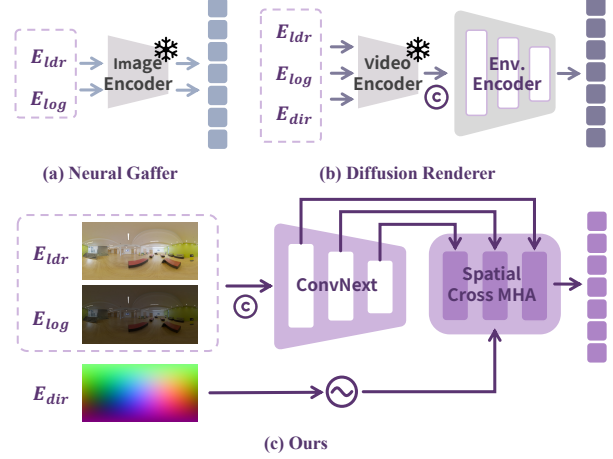


Figure 9. Compared to existing HDRI encoding methods, we bind directional information with multi-scale features using positional encoding.

into a video latent space of consecutive frames, thereby accommodating subsequent image or video diffusion model training.

The lighting-aware tokenizer,  $\mathcal{E}_l$ , is primarily designed to process and inject lighting information into the network to enable relighting while also effectively perceiving rotations in the environment map. Similar to Neural Graffer and Diffusion Renderer, as depicted in Fig. 9, our approach leverages the  $E_{\text{hdr}}$  and  $E_{\text{log}}$  components of environmental illumination to provide lighting color features. Neural Graffer encodes the environment map into the image latent space using a pretrained image VAE’s encoder. Diffusion Renderer, in contrast, employs a video VAE model to compress  $E_{\text{hdr}}$ ,  $E_{\text{log}}$ , and  $E_{\text{dir}}$  into a video latent space of consecutive frames, thus accommodating subsequent image or video diffusion model training. As shown in Fig. 9(c), the design of  $\mathcal{E}_l$  aims to facilitate the injection of lighting information from the LH-SLAT into relightable 3D Gaussian Splatting (GS). This design addresses two key challenges: First, different materials require sensitivity to varying resolutions of lighting information. For instance, highly rough surfaces require only low-resolution environment maps, whereas high-metallicity surfaces with low roughness necessitate high-resolution maps. To address this, we utilize ConvNext [25] to extract multi-resolution features from the lighting pyramid and employ a spatial attention mechanism to compute attention scores and exchange information between these resolutions. Second, the model should accurately perceive rotations of the environment map. Neural Graffer requires deforming the environment map itself. Our approach, similar to Diffusion Renderer, can rotate the illumination by adjusting the environment light direction map,  $E_{\text{dir}}$ , requiring only the application of a rotation matrix to the direction vector. However, Diffusion Renderer relies on an additionally trained environment encoder (Env. En-

coder). Our method employs a direction-encoding-aware spatial cross-multihead attention (Spatial Cross MHA) to guide visual features at different resolutions using directional information. It combines multi-scale feature fusion to preserve both detailed and global information and utilizes a RoPE+RMSNorm transformer layer for efficient sequence modeling, refer to Fig. 3. This allows the complex HDRI lighting information to be encoded into conditional tokens suitable for cross-attention, providing high-quality lighting conditions for the renderer. Abstractly, we model the environment map as a set of light source tokens, each encoded with absolute direction vector positional information and multi-scale features. Subsequently, the Lighting-Aware Decoder (LAD),  $\mathcal{E}_l$ , can efficiently determine the relevance of each token to the current viewpoint by leveraging viewpoint direction encoding.

## B. More Results

### B.1. Additional Comparisons

**Qualitative Evaluation.** We provide comprehensive visual comparisons to further substantiate the effectiveness of our method. Figures 11 and 12 illustrate additional results for single-image reconstruction under diverse illumination conditions. For single-image relighting with unknown input lighting, we present extended comparisons in Figures 13 and 14. Notably, our method recovers significantly more accurate shadows and specular highlights compared to existing 2D diffusion-based relighting models [16, 23, 52, 54], which often struggle with physical consistency.

**Comparison with 3D Generation Baselines.** We also conduct detailed comparisons against state-of-the-art 3D generation methods capable of producing PBR materials [3, 5, 6, 60]. As shown in Fig. 15, our approach demonstrates superior material disentanglement, yielding highlights and tonal values that align closely with the ground truth. To ensure a fair comparison and isolate material quality from geometric failures, we provide the baselines with a fixed frontal view and evaluate the rendered output from the same perspective. This setup mitigates the potential for geometric collapse or severe artifacts in baseline methods, focusing the evaluation on rendering and relighting fidelity.

### B.2. Additional Visualization Results

Leveraging a single input image and a target environment map, our pipeline enables high-fidelity, relightable 3D Gaussian Splatting synthesis with support for multi-view rendering. In Fig. 16, we visualize the decomposed PBR material maps (Albedo, Roughness, Metallic) and the generated shadow maps. These visualizations explicitly demonstrate the effectiveness of our physically-based supervision signals (discussed in Sec. 3.4.2) in achieving clean and plausible material decomposition.



Figure 10. **Failure Cases.** **Left:** High-frequency details (e.g., text) are blurred due to sparse voxel resolution and VAE compression loss. **Right:** Transparent objects exhibit artifacts. While 3DGS theoretically supports transparency via alpha blending, data scarcity leads to inaccurate Gaussian density estimation on surfaces.

## C. Limitations and Future Work

Despite our method’s robust performance in generalized single-image to relightable 3D Gaussian synthesis, several limitations remain.

First, the reconstruction of high-frequency details is bottlenecked by the bottleneck of feature compression. The semantic features extracted by DINOv2 [31] undergo significant downsampling and compression via the VAE encoder to fit within the constrained resolution of the LH-SLAT voxel grid. This process inevitably results in information loss, which is particularly evident in objects with intricate textures, such as the blurred text on the magazine cover shown in Fig. 10 (Left). Future work will explore higher-resolution grids or multi-scale feature refinement strategies to better preserve fine-grained details.

Second, handling transparent materials remains a challenge. Standard PBR workflows typically rely on an alpha channel or a transmission map to render transparency, which most reconstruction methods fail to estimate accurately. While our neural rendering approach inherently supports semi-transparency through the alpha-blending mechanism of 3D Gaussians, it is heavily dependent on data distribution. The scarcity of high-quality transparent objects in our training dataset results in poor supervision for these surfaces. Consequently, the model fails to densify enough Gaussians to form a continuous surface, leading to the checkerboard-like artifacts observed in the glass vase in Fig. 10 (Right). We plan to address this by enriching the training data with transparent objects or designing specialized loss functions for transmission in future work.

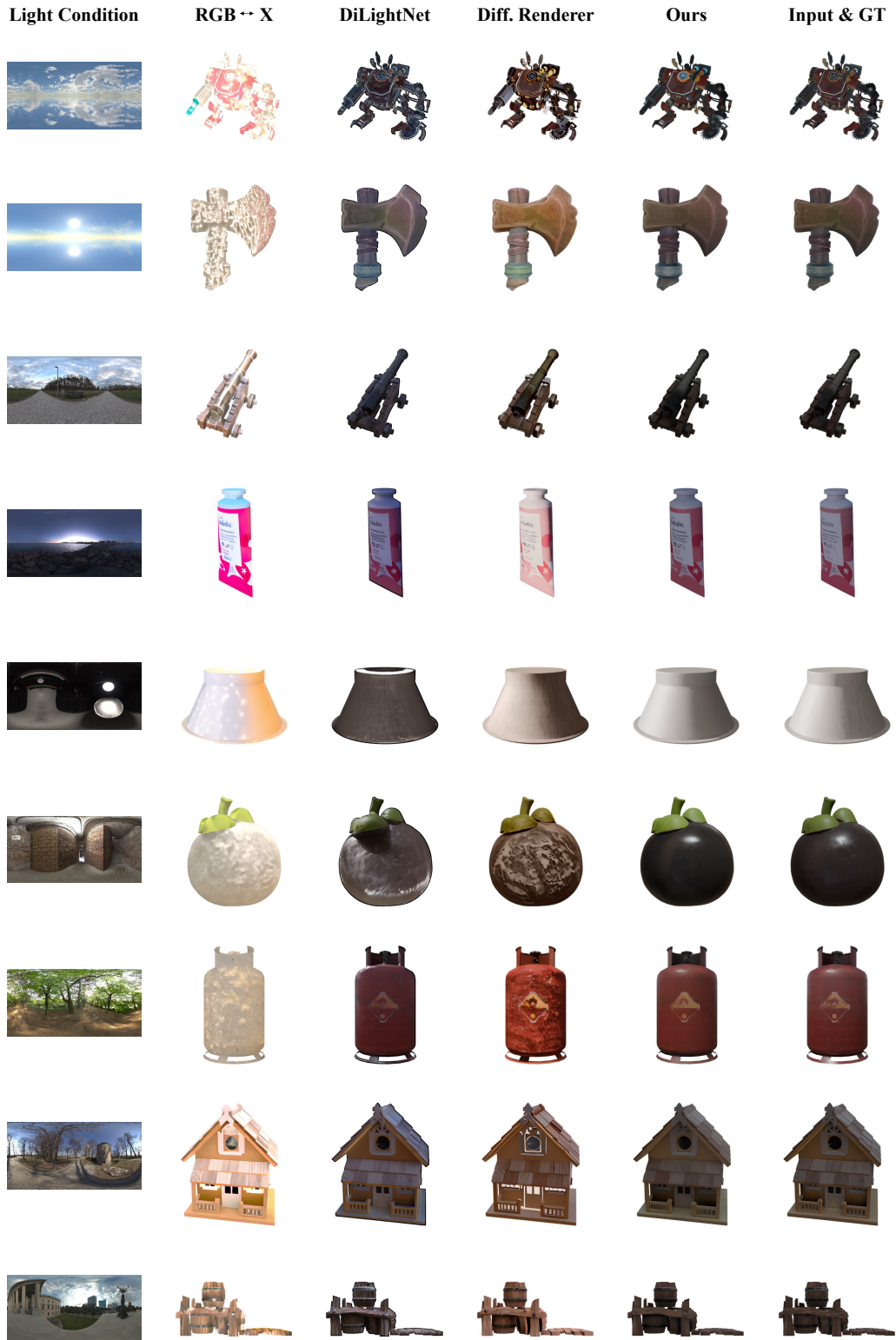


Figure 11. Additional qualitative results for single-image reconstruction under random illumination.

Light Condition	RGB $\leftrightarrow$ X	DiLightNet	Diff. Renderer	Ours	Input & GT
					
					
					
					
					
					
					
					
					

Figure 12. Additional qualitative results for single-image reconstruction under random illumination.

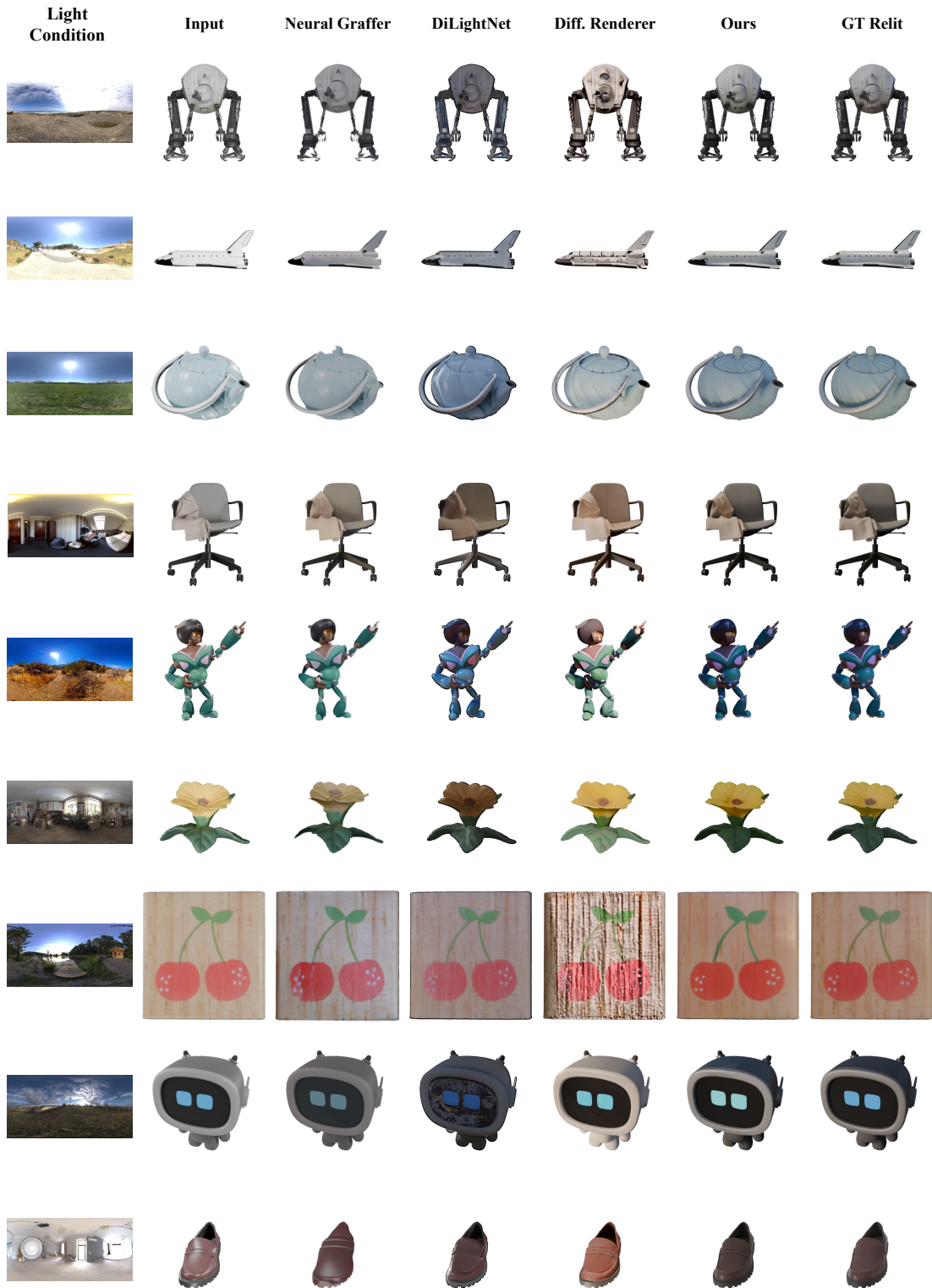
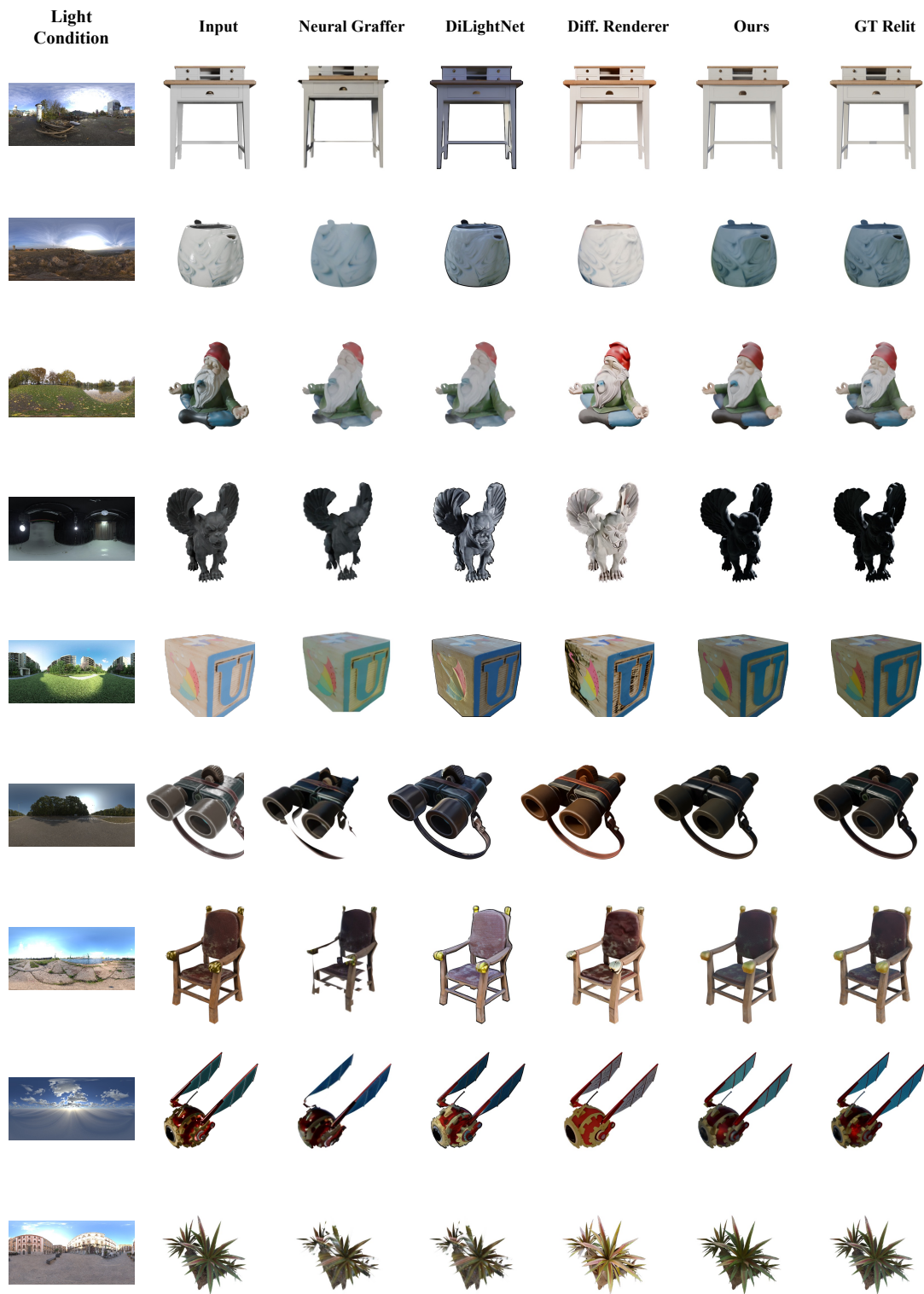


Figure 13. More visualization results of relighting and rendering from a single image under unknown illumination.



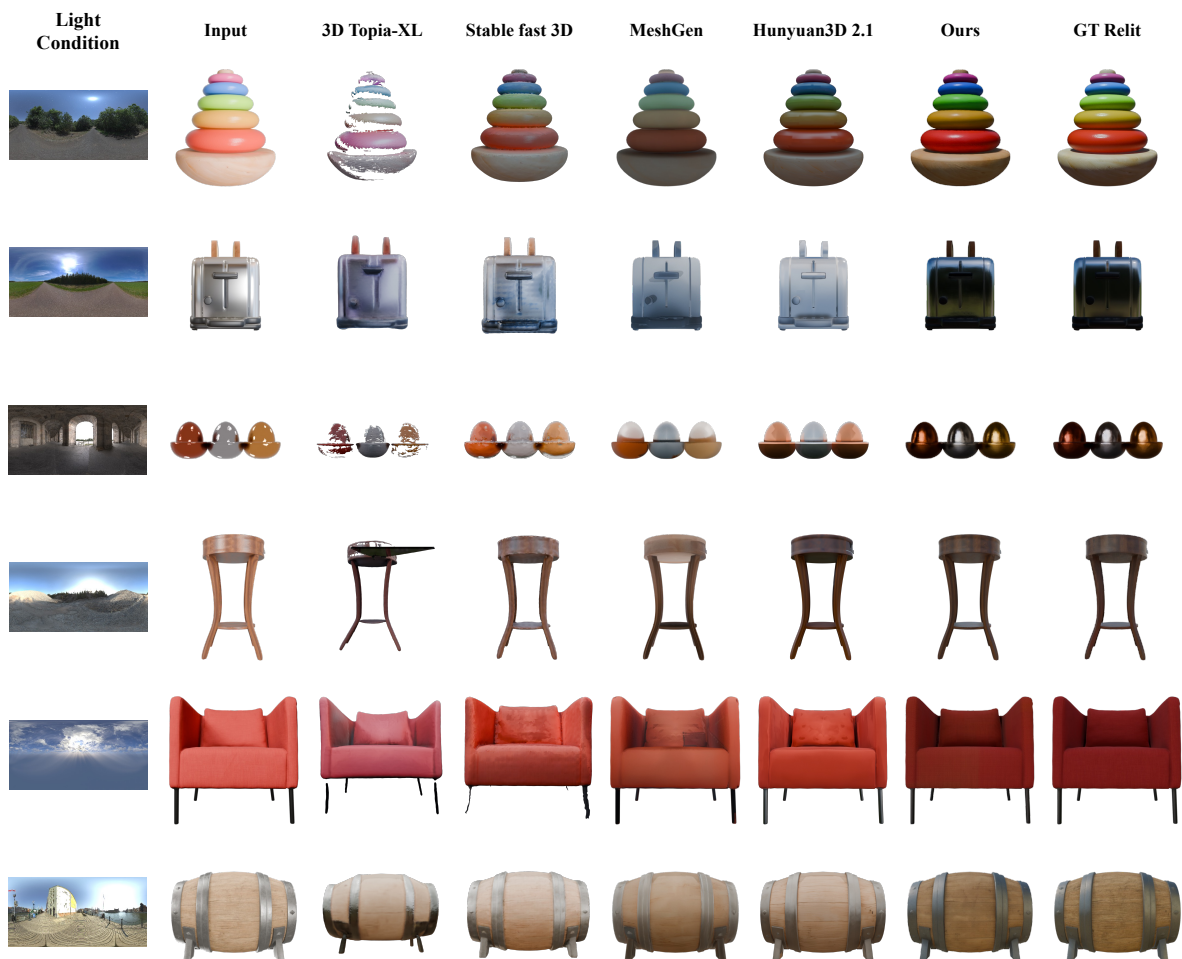


Figure 15. Comparison of relighting renderings between our neural rendering method and 3D generation methods that can recover PBR material properties. Our method achieves more stable and accurate rendering results.



Figure 16. Additional relighting results from a single image under target illumination, along with the PBR materials and shadows estimated by our method.